A SIMPLIFIED PHYSICS AIRFLOW MODEL FOR EVALUATING WIND POWER SITES IN COMPLEX TERRAIN

by

Russell G. Derickson
Robert N. Meroney

for

Summer Computer Simulation Conference
July 18-20, 1977
Hyatt Regency
Chicago, Illinois

The Support of ERDA Grant EY-76-S-06-2438
is Gratefully Acknowledged.

Fluid Mechanics and Wind Engineering Program
Fluid Dynamics and Diffusion Laboratory
Department of Civil Engineering
Colorado State University
Fort Collins, Colorado 80523

March 1977

CEP76-77RGD-RNM31

A SIMPLIFIED PHYSICS AIRFLOW MODEL FOR EVALUATING WIND POWER SITES IN COMPLEX TERRAIN

Russell G. Derickson
Go-Flow Consulting, Fort Collins, Colorado 80521

Robert N. Meroney
Colorado State University, Fort Collins, Colorado 80523

INTRODUCTION

Increasing evidence suggests that numerical simulations may provide the most accurate and economical means for the assessment of prospective wind power generation sites, especially for regions with irregular terrain. Such regions often yield the most desirable locations for wind power extraction due to terrain induced speed up effects, but are elusive to analyze. Depending on general terrain characteristics, atmospheric stability, surface heating, and upstream velocity profiles, the optimum wind locations can be anywhere from the topographic summits to the adjacent valleys. Evaluation by field measurements programs, however, can be quite extensive and costly for each prospective site within a given area, and often misleading in the face of variable meteorological conditions. A well-designed numerical simulation, on the other hand, can more readily and economically point out all potentially favorable sites and effectively determine the separate influences of the various mechanisms modifying the wind. Thus it also seems reasonable that a set of general criteria for wind power siting could be established through a comprehensive numerical simulation program.

A simplified physics airflow model has been developed to handle arbitrary specification of topography and a wide range of meteorological conditions. Initial results show excellent agreement with wind tunnel measurements. A present status comparison to similar models indicates a superiority in both computational results and speed, suggesting potential use in an operational mode. Development goals propose to extend the margin of applicability and refinement of the present model.

DESCRIPTION OF THE MODEL EQUATIONS

Essentially, the model consists of a fully coupled, nonlinear system of steady state momentum and energy equations in which the physics are simplified by neglecting viscosity and explicit turbulence. The two-dimensional version of the model employs a stream function-vorticity approach which is more convenient than the primitive momentum equations for 2-D. However, the 3-D version, still under development, requires use of the momentum equations since a stream function, in the usual sense, does not apply to 3-D. Roache (1) gives examples of analog use of a stream function-vorticity system in 3-D, but the resulting equations become more cumbersome than we feel is warranted.

The 2-D equations of the model are

$$\nabla^2\psi = -\eta \qquad [1]$$

$$\frac{\partial}{\partial x}\left(\frac{\eta\partial\psi}{\partial z}\right) - \frac{\partial}{\partial z}\left(\frac{\eta\partial\psi}{\partial x}\right) = \frac{g}{\theta}\frac{\partial\theta'}{\partial x} \qquad [2]$$

$$\frac{\partial}{\partial x}\left(\frac{\theta'\partial\psi}{\partial z}\right) - \frac{\partial}{\partial z}\left(\frac{\theta'\partial\psi}{\partial x}\right) = 0 \qquad [3]$$

in which ψ is stream function, $u = \frac{\partial\psi}{\partial z}$, $w = \frac{-\partial\psi}{\partial x}$, η is vorticity, and θ' is the potential temperature deviation from an adiabatic atmosphere of constant θ. The present model is of a dry atmosphere, but extention to a moist one would be a relatively simple task and is one of our developmental goals. Moist processes furthermore, are beyond the scope of immediate interest.

A terrain following spatial transformation has been incorporated to eliminate the difficulties associated with finite difference grids and the specification of arbitrary topography (see Fig. 1). The transformation also serves to improve lower boundary condition treatment and to provide a natural method for initializing the model such that solution convergence is dramatically enhanced. Similar to Gal-Chen and Somerville (2), the transformation is given by

$$\bar{x} = x, \quad \bar{z} = \frac{H(z-z_s)}{(H-z_s)} \qquad [4]$$

where $z_s(x)$ is the varying topography, and H is the height at the top of the grid. A schematic of the transformation is shown in Fig. 2.

The transformed equation set, in numerically conservative form, becomes

$$\frac{\partial}{\partial\bar{x}}\left(\frac{\partial\sqrt{G}\psi}{\partial\bar{x}}\right) + \frac{\partial}{\partial\bar{x}}\left(\frac{\partial\sqrt{G}\,G^{13}\psi}{\partial\bar{z}}\right) + \frac{\partial}{\partial\bar{z}}\left(G^{13}\frac{\partial\sqrt{G}\psi}{\partial\bar{x}}\right) + \frac{\partial}{\partial\bar{z}}\left(G^{13}\frac{\partial\sqrt{G}\,G^{13}\psi}{\partial\bar{z}}\right) + \frac{1}{\sqrt{G}}\frac{\partial}{\partial\bar{z}}\left(\frac{\partial\psi}{\partial\bar{z}}\right) = -\sqrt{G}\,\eta \qquad [5]$$

$$\frac{\partial}{\partial\bar{x}}\left(\eta\frac{\partial\psi}{\partial\bar{z}}\right) - \frac{\partial}{\partial\bar{z}}\left(\eta\frac{\partial\psi}{\partial\bar{x}}\right) = \frac{g}{\theta}\left[\frac{\partial}{\partial\bar{x}}(\sqrt{G}\theta') + \frac{\partial}{\partial\bar{z}}(\sqrt{G}\,G^{13}\theta')\right] \qquad [6]$$

$$\frac{\partial}{\partial\bar{x}}\left(\theta'\frac{\partial\psi}{\partial\bar{z}}\right) - \frac{\partial}{\partial\bar{z}}\left(\theta'\frac{\partial\psi}{\partial\bar{x}}\right) = 0 \qquad [7]$$

with the velocity components defined as

$$u = \frac{1}{\sqrt{G}}\frac{\partial\psi}{\partial\bar{z}}, \quad w = -\frac{1}{\sqrt{G}}\left(\frac{\partial\sqrt{G}\psi}{\partial\bar{x}} + \frac{\partial\sqrt{G}\,G^{13}\psi}{\partial\bar{z}}\right) \qquad [8]$$

in which

$$\sqrt{G} = 1 - z_s/H, \text{ and } G^{13} = \frac{1}{\sqrt{G}}\left(\frac{\bar{z}}{H} - 1\right)\frac{\partial z_s}{\partial\bar{x}}$$

In 3-D, the same transformation is extended whereby z_s becomes a function of the two horizontal coordinates x and y, i.e. $z_s(x,y)$.

To further enhance the model, horizontal and vertical grid expansions are included in the transformed $\bar{x}$ - $\bar{z}$ system.

The vertical expansion economically provides for greater resolution near the topographic surface where it is needed, while allowing for the top boundary to be placed sufficiently far from the surface as to minimize any undesirable numerical boundary interference. Similarly, the horizontal expansion serves to retract the lateral boundaries from the terrain in as few grid points as possible. The composite effect is shown in Fig. 3. The functional forms of the expansions are

1) vertical: $\bar{z} = \xi_v^p$, $1 \leq p \leq 2$ [9]

2) horizontal: $\bar{x} = C_o(b\xi_h^4 + \xi_h)$ (downstream of terrain) [10a]

$$\bar{x} = C_o[b-b(1-\xi_h)^4 + \xi_h]$$ (upstream of terrain) [10b]

in which the constant b determines the magnitude of the expansion and C_o corresponds to the uniform horizontal grid spacing bordering the expansion. The forms of equations [5]-[8] are somewhat modified by expansions [9] and [10], the details of which are not crucial to this paper and, therefore, will not be shown (e.g., see De Rivas (3)).

The single disadvantage of greater complexity in the transformed equations is far outweighed by the many advantages gained, not the least of which is a saving in computational time. This is borne out by experience with comparable solutions in the usual Cartesian framework versus the transformed coordinate approach.

CONCEPT AND RATIONALE OF THE MODEL

Upstream temperature and wind shear are specified along with surface temperature and an implicit no-slip momentum condition to drive the steady state inviscid algorithms toward a simulated viscous solution. Conceptually, the model provides topographically induced modifications to upwind temperature and velocity profiles which correspond to an equilibrium state achieved through viscous and turbulent processes. The tacit assumption is that the viscous and turbulent mechanisms play secondary roles to advective momentum and thermal transport, for the relevant time scales being simulated as the wind flows over the terrain.

Thwaites (4) has reviewed early literature on the solution of inviscid equations of motion for shear flow over two- and three-dimensional surface disturbances (see Lighthill (5) and Hawthorne and Martin (6)). The success of this approach suggests that an inviscid flow field with the appropriate approach velocity profile may satisfactorily estimate windfields over terrain.

Scorer (7) defends the use of inviscid equations to model turbulent wind profiles over mountainous terrain as long as the conditions for flow separation do not arise. Sensitivity studies by Fosberg (8) indicate that topography and thermal stratification dominate wind patterns with friction exerting only a minor influence. However, it is felt by this author that the modeling of large or sudden changes in surface roughness and strong surface heating, with the eventual inclusion of separation, will necessitate the addition of a turbulent sublayer to the present model. Such a sublayer would be shallow compared to the total depth of the model, so the added complexity, while improving results, would not appreciably affect computational speed.

NUMERICAL ALGORITHMS AND SOLUTION

Equations [5]-[7], as modified by [9] and [10] are central-differenced and manipulated into steady state algorithms. Equations [6] and [7] are treated somewhat differently than [5] in that they are differenced with respect to an inter-node location so as to prevent an uncoupling in the resulting scheme. (All variables reside at the same node locations.) Equation [5] takes the form of a successive-over-relaxation algorithm, whereas [6] and [7] become simple spatial marching algorithms consistent with their hyperbolic nature. A solution is obtained very quickly in which the equations are completely coupled during each iteration.

Equations [6] and [7] both require specification of values at the inflow boundary, whereas outflow values determine themselves. The lower boundary value of vorticity is not needed in [6] since ψ vanishes at the surface and there is no viscosity; likewise for θ' in [7] except that it is needed in [6] in the last term on the right hand side and is therefore specified. There appears to be some inconsistency in usage of the surface value of θ' that implies further investigation. At the top boundary, events are handled in two ways. For a rigid lid, θ' and η are held constant. In the case of a so-called flexible lid, η is held constant and θ' conforms to the condition $\partial^2\theta'/\partial z^2 = 0$.

Equation [5], being elliptic, requires either Dirichlet or Neumann specification at each boundary. Inflow, outflow, and surface values are specified as Dirichlet conditions, the surface value being zero. Since incoming velocity and temperature drive the solution, ψ is determined by integrating the inflow velocity profile which is given as a power function to simulate the types of shear observed in the atmosphere. Outflow values of ψ are the same as the corresponding inflow values. Along the upper boundary, ψ is either constant for a rigid lid or satisfies the Neumann condition $\partial\psi/\partial z = U(x)$ for a flexible lid.

Since the equations are fully nonlinear and coupled, the solution is physically complete with the exception of the lack of viscosity and turbulence, for which several justifications have been presented. Comparative results to wind tunnel testing confirm the validity of the numerical simulation and suggest a strong potential for operational and research application. The future of a 3-D inviscid model seems particularly bright.

RESULTS AND DISCUSSION

Comparison to Wind Tunnel Measurements

A direct comparison between the numerical simulation model and wind tunnel measurements (Meroney, et al. (9)) was made for neutrally stratified flow over sinusoidal hills with mean slopes of 1:3 and 1:4. Figures 4 and 5 show these comparative results in normalized form. Representative contour plots are shown in Figs. 6 and 7.

The numerical model shows remarkable agreement with the wind tunnel data, especially for the 1:4 hill. Somewhat less agreement occurs for the 1:3 hill case and the discrepancy is caused in part by differences in the upstream wind profile shapes of the wind tunnel versus the numerical model. In the wind tunnel, the data corresponding to inflow values for the 1:3 hill were taken at $x/L = -4$ (L is the half-width of the hill; $x = 0$ is at the summit) and do not conform as precisely to the wind profile power law, $\frac{U}{U_{ref}} = (\frac{Z}{Z_{ref}})^{\alpha}$, as does the 1:4 hill case in which inflow data were taken at $x/L = -5$. In general, a power law is quite accurate in describing the velocity profile at a sufficiently large distance upstream of an obstacle. Better agreement and an improved evaluation between wind tunnel and numerical results could be expected for the 1:3 hill case if the numerical solution employed a spline fit, for example, to replicate the inflow values of the wind tunnel which are not far enough upstream to obey the power law. Another cause for discrepancy is that the relatively steep 1:3 hill creates a leeward effect in the wind tunnel associated with turbulence which feeds back upstream, whereas the inviscid numerical model cannot simulate turbulence production.

The use of a rigid lid, i.e. ψ = constant at the top of the grid, versus a flexible one in which $\partial\psi/\partial z = u(x)$ at grid top, revealed some interesting simulation results. The top of the numerical model is taken at 10h which is the approximate depth of the boundary layer indicated by the wind tunnel data. h is the elevation of the summit of the hill.

A rigid lid, by virtue of its exaggerated venturi effect, (i.e., the top streamline is constrained to be horizontal and cannot have upward displacement as would be expected in a real geophysical flow over terrain) should tend to overpredict speedup values. If a rigid lid is employed at 10h, however, the numerical model somewhat under predicts the speedup observed in the wind tunnel. It would seem, then, that

turbulent mixing must be responsible for the higher wind tunnel values. However, a numerical experiment was performed with a flexible lid, in which u values at 10h were adjusted to wind tunnel data. Although the adjusted u values varied a maximum of only 1 percent greater than corresponding rigid lid values, velocities near the topographic surface were increased by about 2 percent and the model produced much better general agreement with wind tunnel predictions. Thus it appears that the primary speedup mechanism is inviscid and not turbulent.

Another numerical experiment, in which a rigid lid was placed lower than 10h, i.e., at about 5h, resulted in a systematic overprediction of wind tunnel measurements. It becomes clear that placement of the numerical rigid lid somewhere between 5h and 10h would result is almost exact agreement with the wind tunnel. This leads to the suggestion that the wind tunnel is producing an effective rigid lid at a height lower than 10h, even though the top of the tunnel is much higher than 10h. The probable cause of this effect is that the boundary layer growing along the top of the tunnel is producing a subtle interference with the upper portions of the underlying airstream.

The composite experience of wind tunnel and numerical experimentation provides a rational basis for treatment of the upper boundary in the numerical model. The conclusion we have come to, after additional numerical experiments, is that the flexible lid with $\partial\psi/\partial z = U$, in which U is a constant free-stream value, produces the most consistent behavior of ψ, particularly near the top boundary. This freestream condition is valid only if the top boundary is placed sufficiently above the topography. What is sufficient is largely a matter of numerical experimentation for specific cases, but can perhaps be generalized at a later date.

Preliminary Results With Stratified Flow

Some comparative numerical experiments were performed with stable, neutral, and unstable stratification. (At this time there are no wind tunnel data for stable or unstable flow.) Mild stability tends to decrease the speedup factor, whereas mild instability for a given approach velocity profile tends to increase the speedup factor. This agrees with the energy analysis proposed by Lange (10). Sacre (11, 12) noted similar behavior in his numerical model and an inverse behavior in his analytic model. As opposed to our inviscid model, neither his analytic or numerical model appears to account for modifications on stability as the flow transects the topography. Additionally, Sacre's and similar models are restricted to very small departures from neutral stability, i.e., $R_i \sim 0(0)$, whereas our model can handle significantly greater ranges in stability, including mild inversions. Microfilmed plots of preliminary experiments with stratification are shown in Figs. 8 and 9. A summary of results is given in Tables 1 and 2.

An interesting observation is that the 1:3 sinusoidal hill produces less marked variations in speedup behavior for changes in thermal stratification than does the 1:4 hill, although the 1:3 hill produces consistently greater speedup values in general. Also, for both the 1:3 and 1:4 cases, there is a significant difference between a rigid and flexible lid for stable stratification which becomes negligibly small with decreasing stability.

In summary, the numerical simulation model has demonstrated its ability to handle a wide range of thermal stratification in which the Richardson number deviates significantly from 0, i.e., $|Ri| \gg 0$. However, the model is not capable of simulating lee-wave or blocking behavior on the one extreme, or free-convection on the other. The present model is being further developed to include the lee-wave case, a matter primarily of appropriate boundary treatment.

Solution Speed

The model appears significantly faster than other models. Neutral flow requires slightly over 2.0 seconds and stratified flow about 3.0 seconds, on a CDC-7600. Deaves (13), for example, cites his time requirement for neutral flow as 5 to 20 minutes on a machine comparable to a CDC-6400. A CDC-7600 is about 15 times faster than a CDC-6400, so the speed advantage over Deaves is in the range of about 10 to 40 times greater.

SUMMARY

The simplified physics model presented herein displays a number of advantages in realism and computational speed over similar numerical models. The use of an inviscid approximation has led to the understanding that speedup is primarily an inviscid mechanism, with friction, i.e., viscosity or turbulence acting only to modify the basic effect. For many situations, friction does not have time to produce significant changes in the wind flowing over complex terrain and an inviscid model is quite justified.

Comparison with wind tunnel measurements provides verification of the validity of the numerical simulation model. Its eventual use as an operational tool to help locate optimum wind power generation sites in complex terrain seems quite likely. A comprehensive simulation program for establishing general siting criteria is one of the goals envisioned in the development of the present model.

ACKNOWLEDGMENTS

The support of U.S. Energy Research and Development Administration Contract EY-76-S-06-2438 and the National Center for Atmospheric Research Computing Facility are gratefully acknowledged.

REFERENCES

1. Roache, Patrick J., Computational Fluid Dynamics, Hermosa Publishers, Albuquerque, 1972.
2. Gal-Chen, T. and Somerville, R. C. J., "On the Use of a Co-Ordinate Transformation for the Solution of the Navier-Stokes Equations," J. Computational Physics, Vol. 17, pp. 209-228, 1975.
3. DeRivas, Eugenia Kalnay, "On the Use of Nonuniform Grids in Finite-Difference Equations," J. of Comp. Phys., Vol. 10, pp. 202-210, 1972.
4. Thwaites, B., Incompressible Aerodynamics, Clarenoon Press, Oxford, 636 p., 1960.
5. Lighthill, M. J., "The Fundamental Solution for Small Steady Three-Dimensional Disturbances to a Two-Dimensional Parallel Shear Flow," J. Fluid Mechanics, Vol. 3, pp. 113-144, 1957.
6. Hawthorne, W. R. and Martin, M. E., "The Effect of Density Gradient and Shear on the Flow Over a Hemisphere," Proc. Royal Soc. A, Vol. 232, pp. 184-195, 1955.
7. Scorer, R. S., "Theory of Airflow Over Mountains. IV: Separation of Airflow from the Surface," Quart. J. R. Met. Soc., 81, pp. 340-350, 1955.
8. Fosberg, M. A., Marlatt, W. E., and Krupnak, L., "Estimating Airflow Patterns Over Complex Terrain," USDA Forest Service Research Paper RM-162, Rocky Mountain Forest and Range Experiment Station, Fort Collins, Colorado, 1976.
9. Meroney, R. N., Sandborn, V. A., Bouwmeester, R. J. B., and Rider, M. A., "Sites for Wind Power Installations: Wind Tunnel Simulation of the Influence of Two-Dimensional Ridges on Wind Speed and Turbulence - Tabulated Experimental Data - Progress Report for the Period June - November 1976," Colorado State University, Fort Collins, Report No. CER76-77RNM-VAS-RB-MAR29, December 1976.
10. Lange, K. O., "Some Aspects of Site Selection for Wind Power Plants on Mountainous Terrain," Proceedings of the UN Conference on New Sources of Energy Resources, 7, pp. 125-128, August 21-31, 1961.
11. Sacre, C., "Theoretical Estimation of the Properties of Airflow Over a 2-Dimensional Hill," Centre Scientifique et Technique du Batement, Nantes, France, 30 p., 1974.
12. Sacre, C., "Numerical Method for Near Calculation of the Excess Velocity of the Wind on a Hill," Centre Scientifique et Technique du Batement, Nantes, France, 26 p., 1975.
13. Deaves, D. M., "Wind Over Hills--A Numerical Approach," Environmental Sciences Research Unit, Cranfield Institute of Technology, United Kingdom, 30 p., May 1975.

Table 1. Preliminary numerical results with thermal stratification over 1:4 sinusoidal hill. The speedup factor, S, is defined as the ratio of the wind speed at a height Δz above the terrain summit to the inflow windspeed at a height equal to the summit plus Δz; in other words, the compared velocities are at the same absolute altitude. Δz was chosen as 0.028H and corresponds to the point of maximum speedup. H is the grid top elevation.

bulk stratification parameter, $\frac{H}{\theta}\frac{\partial \theta'}{\partial z}$	stability classification	power law, α	type of upper boundary	speedup factor, S
0.00732	stable	0.13	flexible lid	1.128
0.00366	stable	0.13	flexible lid	1.172
0	neutral	0.13	flexible lid	1.198
-0.00366	unstable	0.13	flexible lid	1.215
-0.00732	unstable	0.13	flexible lid	1.226
0.00732	stable	0.13	rigid lid	1.206
0.00366	stable	0.13	rigid lid	1.214
0	neutral	0.13	rigid lid	1.221
-0.00366	unstable	0.13	rigid lid	1.226
-0.00732	unstable	0.13	rigid lid	1.230

Table 2. Preliminary numerical results with thermal stratification over 1:3 sinusoidal hill. The speedup factor, S, is defined as the ratio of the wind speed at a height Δz above the terrain summit to the inflow windspeed at a height equal to the summit plus Δz; in other words, the compared velocities are at the same absolute altitude. Δz was chosen as 0.028H and corresponds to the point of maximum speedup. H is the grid top elevation.

bulk stratification parameter, $\frac{H}{\theta}\frac{\partial \theta'}{\partial z}$	stability classification	power law, α	type of upper boundary	speedup factor, S
0.00732	stable	0.13	flexible lid	1.255
0.00366	stable	0.13	flexible lid	1.273
0	neutral	0.13	flexible lid	1.286
-0.00366	unstable	0.13	flexible lid	1.293
-0.00732	unstable	0.13	flexible lid	1.300
0.00732	stable	0.13	rigid lid	1.287
0.00366	stable	0.13	rigid lid	1.292
0	neutral	0.13	rigid lid	1.296
-0.00366	unstable	0.13	rigid lid	1.299
-0.00732	unstable	0.13	rigid lid	1.301

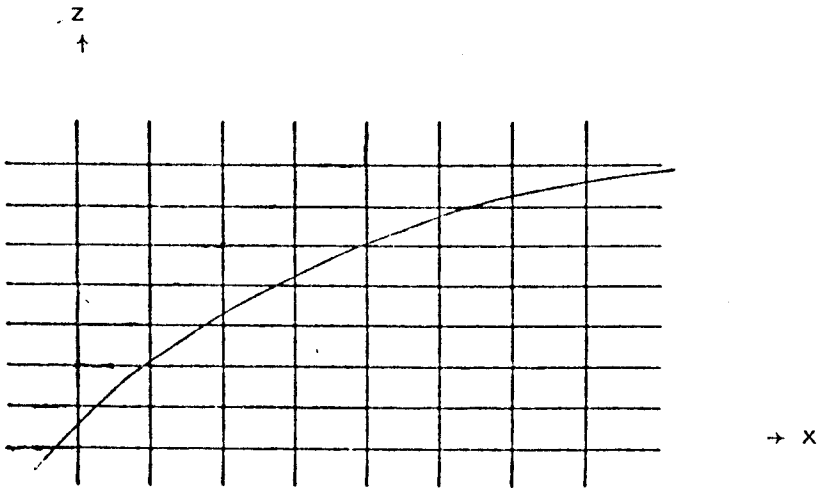

Figure 1. Example of irregular grid spacing at the surface, associated with arbitrary terrain specification in a cartesian x-z system. In general the terrain does not conform to grid nodes.

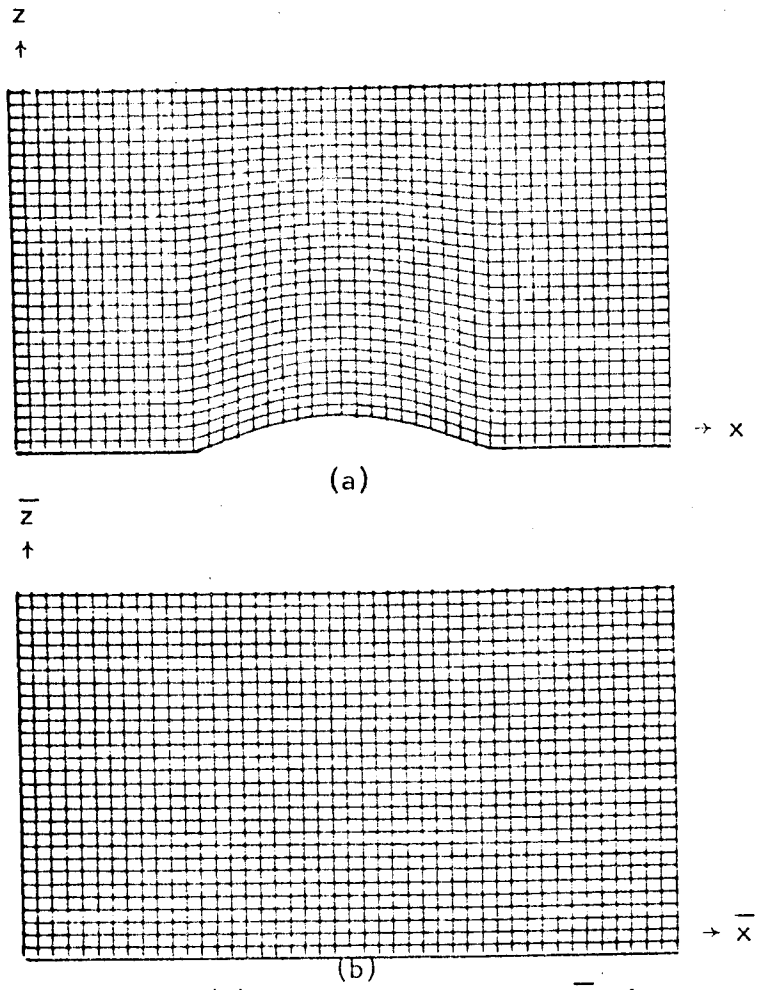

Figure 2. (a) Lines of constant $\bar{z}$, i.e. z transformed, in the original x-z system. (b) Lines of constant $\bar{z}$ in the $\bar{x}$-$\bar{z}$ system. The computational domain becomes a simple rectangle. In 3-D the domain becomes a box.

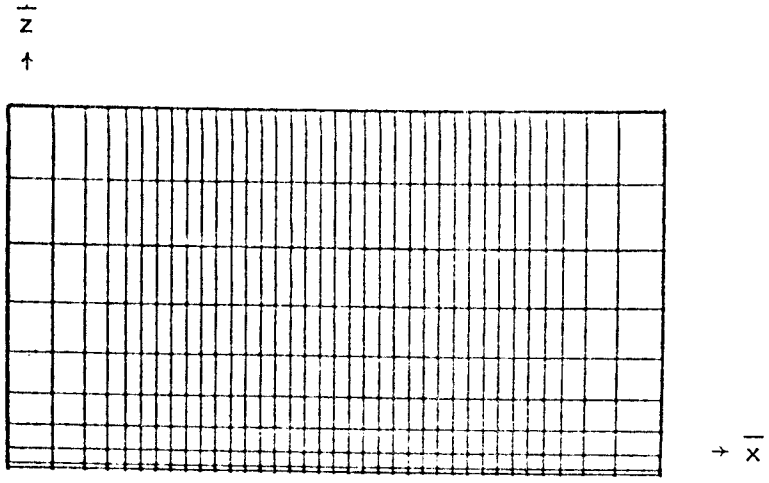

Figure 3. Schematic of horizontal and vertical grid expansions within $\bar{x}$-$\bar{z}$ system. Spatial resolution is improved where needed, while minimizing the required number of grid nodes.

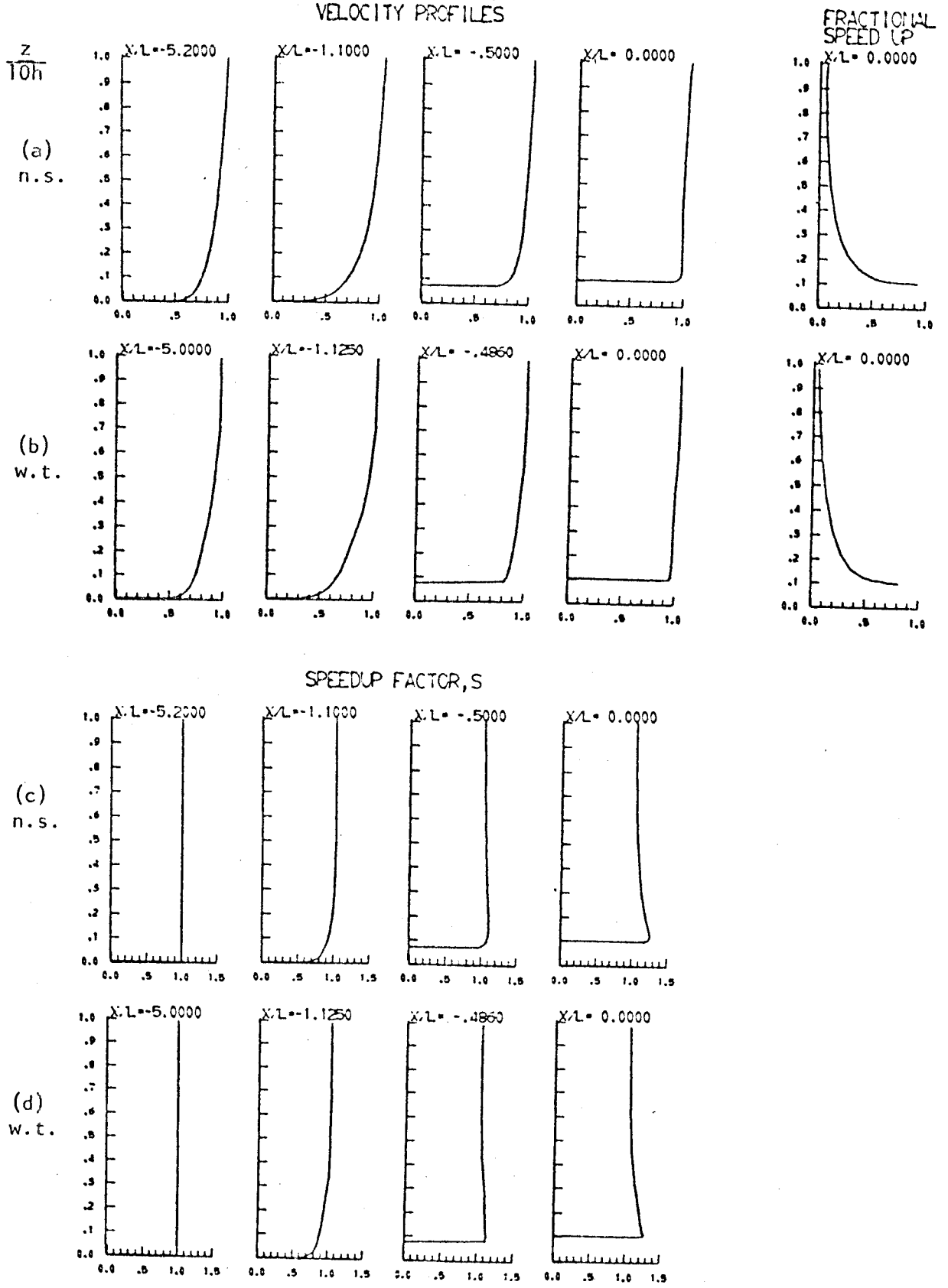

Figure 4. Comparison between wind tunnel data (w.t.) and numerical simulation (n.s.) results for a 1:4 sinusoidal hill. Velocities are normalized with respect to the inflow velocity at 10h, where h is the elevation at the hill summit. Speedup is defined as the ratio of the horizontal velocity, u, at a given elevation over the terrain to the inflow u value at the same elevation. Fractional speedup is defined by $[U_o(z+h)/U_i(z)]-1$ in which $U_o(z+h)$ lies above the summit and $U_i(z)$ is at the inflow boundary. x/L is the ratio distance upstream of the summit. L is the half-width of the hill.

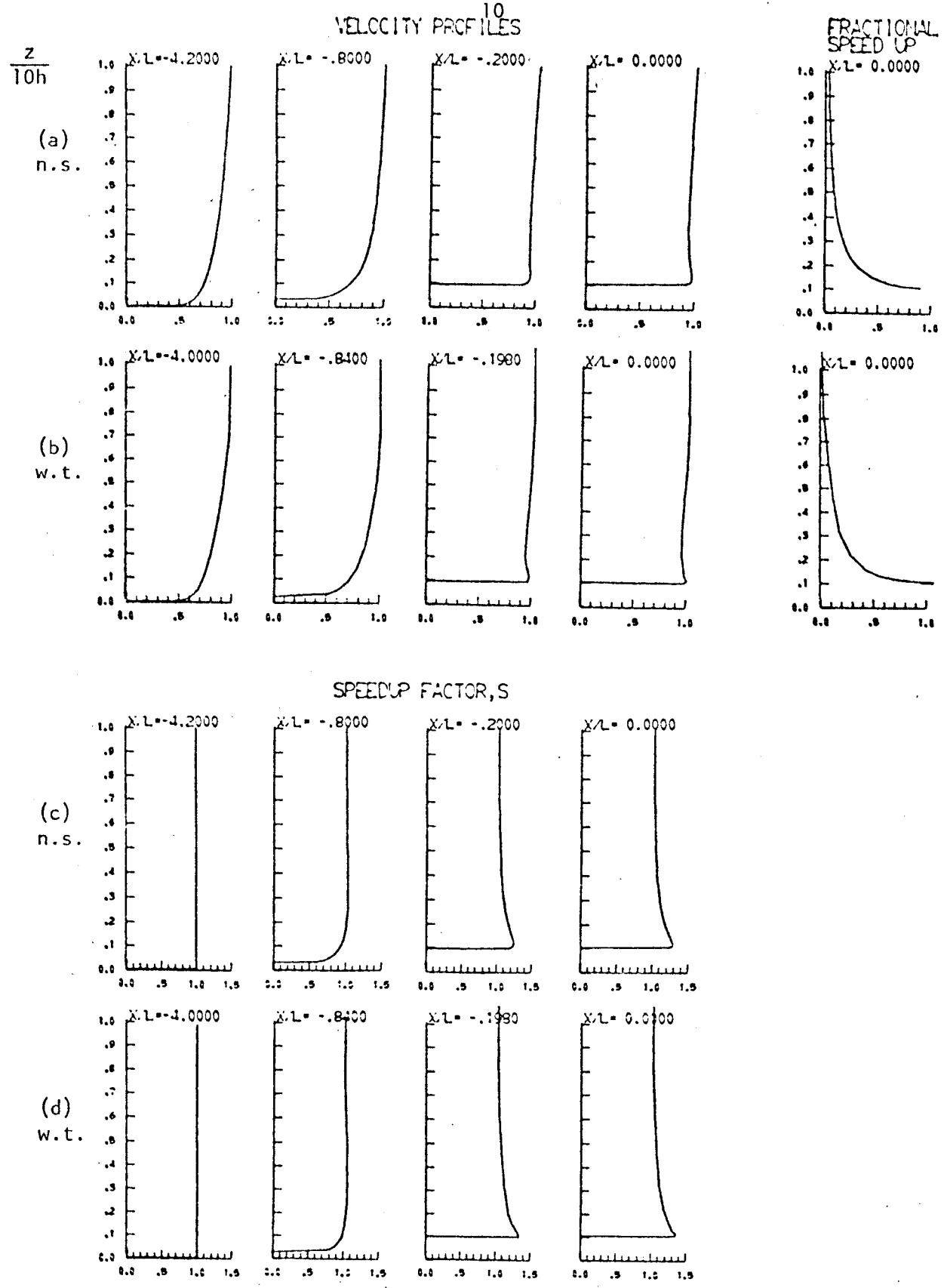

Figure 5. Comparison between wind tunnel data (w.t.) and the numerical simulation model (n.s.) for a 1:3 sinusoidal hill. Definitions are given in Figure 4.

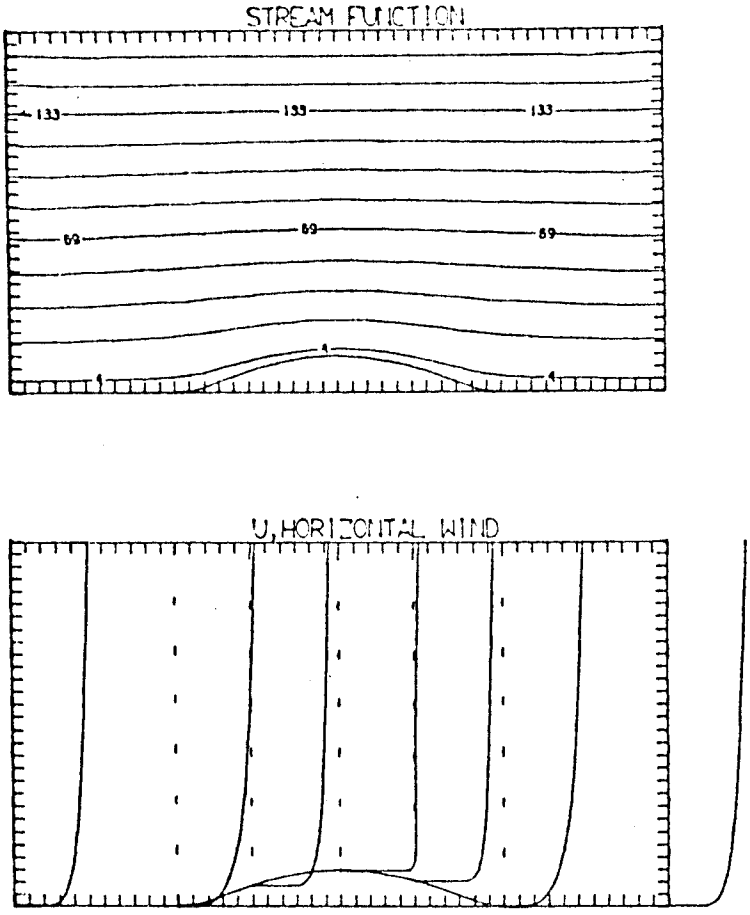

Figure 6. Contour plots of numerical simulation results for neutral flow over a 1:4 sinusoidal hill. These plots correspond to n.s. graphs of Figure 4 and help to illustrate the character of the velocity speedup. Vertical and horizontal scales are correct except near the lateral boundaries where a grid expansion was employed.

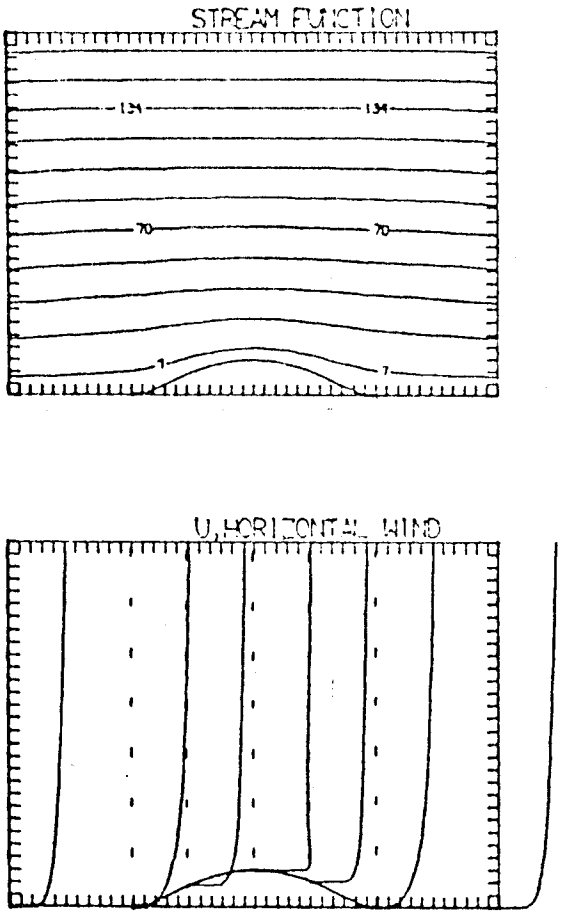

Figure 7. Contour plots of numerical simulation results for neutral flow over a 1:3 sinusoidal hill. These plots correspond to n.s. graphs of Figure 5 and help to illustrate the character of the velocity speedup. Vertical and horizontal scales are correct except near the lateral boundaries where a grid expansion was employed.

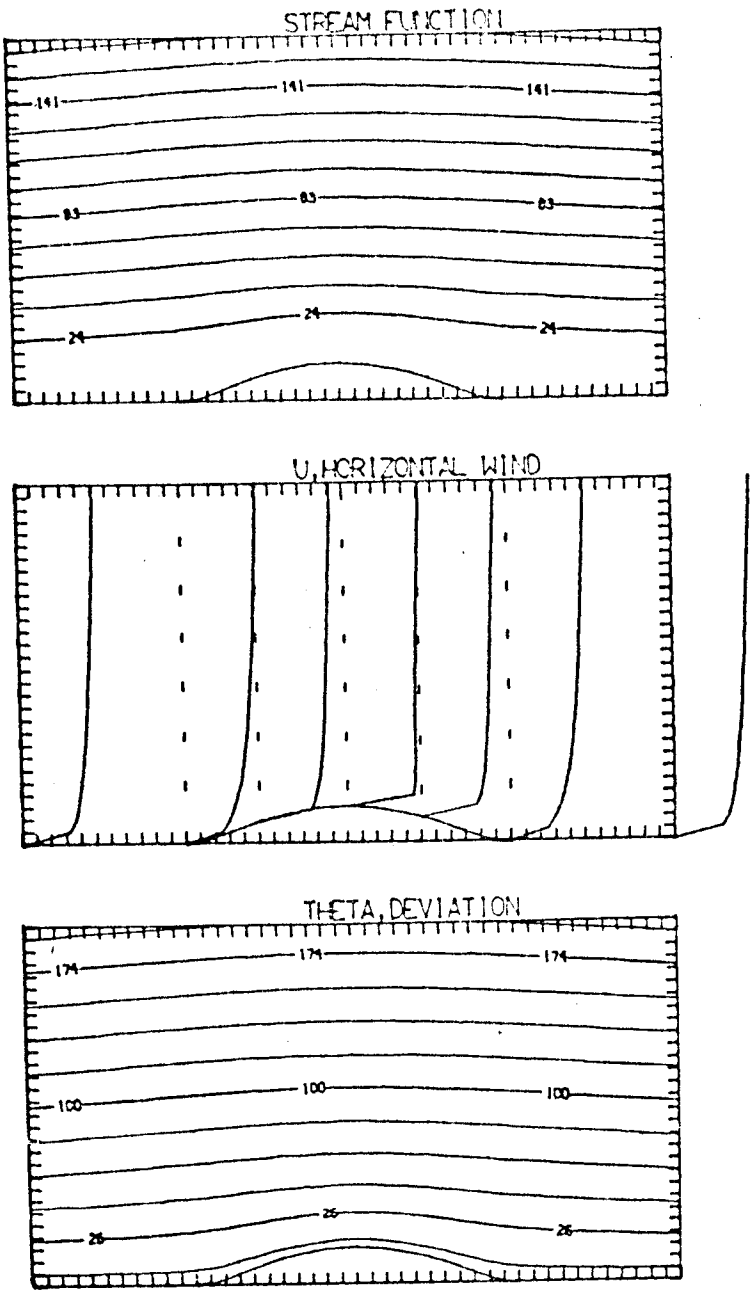

Figure 8. Contour plots of numerical simulation results for stable flow over a 1:4 sinusoidal hill. A flexible lid (see text) was employed. At the top of the grid $\theta' = 2^{\circ}K$. Richardson numbers greatly exceed 1 and no longer have meaningful physical significance. There are no comparative wind tunnel data.

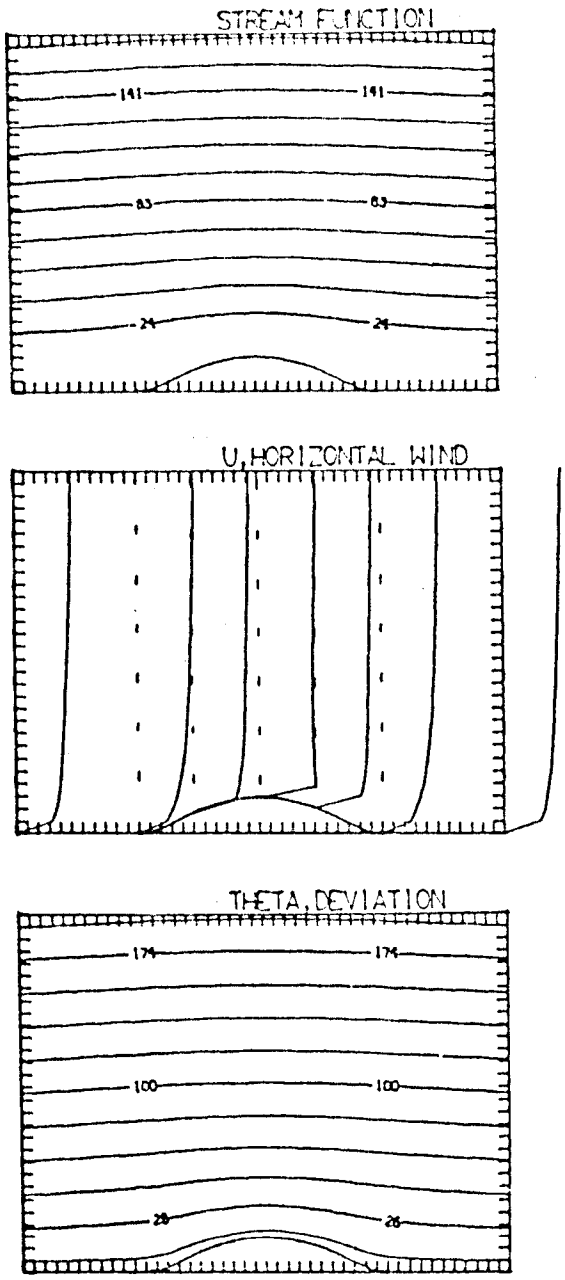

Figure 9. Contour plots of numerical simulation results for stable flow over a 1:3 sinusoidal hill. A flexible lid (see text) was employed. At the top of the grid $\theta' = 2^{o}K$. Richardson numbers greatly exceed 1 and no longer have meaningful physical significance. There are no comparative wind tunnel data.